Journal of Power Sources 242 (2013) 230–235

Contents lists available at SciVerse ScienceDirect

Journal of Power Sources

journal homepage: www.elsevier.com/locate/jpowsour

Synthesis and performance of $Li_{1.5}V_3O_8$ nanosheets as a cathode material for high-rate lithium-ion batteries

Yanli Wang, Xingyan Xu*, Chuanbao Cao*, Cui Shi, Wei Mo, Hesun Zhu

Research Centre of Materials Science, Beijing Institute of Technology, No.5, Zhongguancun South Street, Beijing 100081, PR China

HIGHLIGHTS

- We firstly prepared $Li_{1.5}V_3O_8$ nanosheets by sol–gel method.
- $Li_{1.5}V_3O_8$ nanosheets had smooth surface with typical width of 600 nm, length of 800 nm.
- The initial discharge capacity was 260, 204 mAh g^{-1} at 130 and 175 mA g^{-1}, respectively.
- The discharge capacity was 170, 100 mAh g^{-1} at 130 and 175 mA g^{-1}, respectively, after 100 cycles.

ARTICLE INFO

Article history:
Received 12 December 2012
Received in revised form
9 May 2013
Accepted 15 May 2013
Available online 22 May 2013

Keywords:
Lithium-ion batteries
Lithium vanadate
Sol–gel method
Nanosheets

ABSTRACT

$Li_{1.5}V_3O_8$ nanosheets as a cathode material for high-rate lithium-ion batteries are prepared by sol–gel method. SEM and TEM observations show that the prepared samples are nanosheet structure, with a typical width of 600 nm and length of 800 nm. Charge–discharge measurements demonstrate that $Li_{1.5}V_3O_8$ nanosheets exhibit high initial discharge specific capacity of 260, 204 mAh g^{-1} at current densities of 130 mA g^{-1} and 175 mA g^{-1}, respectively. Even after 100 cycles, the discharge specific capacity still remains 170 mAh g^{-1} and 100 mAh g^{-1}. The high discharge specific capacity and good cycling stability are attributed to nanosheets morphology of $Li_{1.5}V_3O_8$ that can provide lithium ions with more sites, shorten diffusion distance, and maintain good contact between the active material and electrolyte. All these results indicate that $Li_{1.5}V_3O_8$ nanosheets are promising cathode materials for lithium-ion batteries.

1. Introduction

Rechargeable lithium ion batteries are considered as the most advanced electrochemical energy storage and transfer systems in portable devices and hybrid electric vehicles [1]. It is well known that the cathode materials are particularly critical in determining the performance of lithium ion batteries. During the past 30 years, $Li_{1+x}V_3O_8$ has been investigated extensively as a cathode material because of its higher specific capacity, lower cost, and better safety features [2–5]. $Li_{1+x}V_3O_8$ has a layered structure with two basic structural units of VO_6 octahedra and VO_5 distorted trigonal bipyramids [6]. There are two different sites for lithium ions, octahedron and tetrahedron. Lithium ions generally occupy the octahedral sites. As more lithium ions intercalate into the host compound, extra lithium ions may enter the tetrahedral sites. Lithium ions in the octahedral sites link to the V_3O_8 layers via strong ionic bonds, which make the crystal structure of $Li_{1+x}V_3O_8$ stable during the insertion/extraction process. Despite its structural advantages, the prepared methods and processing conditions have significant influences on the crystal structure and electrochemical performances of $Li_{1+x}V_3O_8$. Up to date, numerous methods have been developed to prepare $Li_{1+x}V_3O_8$ with the aim to improve its capacity and stability, such as traditional solid-state reaction [7,8], spray drying method [9], hydrothermal reaction [4], microwave assisted solid-state method [10], [rheological phase reaction method [11] and sol–gel method [12–14]. Furthermore, the structure and morphology as well as particle size of the $Li_{1+x}V_3O_8$ have important effects on its electrochemical properties [4,7–11].

Recent advanced studies of $Li_{1+x}V_3O_8$ materials take care of nanostructured materials with various morphologies such as nanorods [15], nanotube [16], nanosheets [17,18] and nanoparticles [19]. These nanomaterials have improved the performance of lithium batteries to some extent, such as the higher insertion/extraction rates and specific capacity due to their high specific surface area, short diffusion distance for mass and charge transport [15–19]. However, the shape control of $Li_{1+x}V_3O_8$ nanostructures

* Corresponding authors. Tel.: +86 10 68913792; fax: +86 10 68912001.
E-mail address: cbcao@bit.edu.cn (C. Cao).

0378-7753/$ – see front matter © 2013 Elsevier B.V. All rights reserved.
http://dx.doi.org/10.1016/j.jpowsour.2013.05.059

remains a great challenge, which can provide a great opportunity to improve their electrochemical properties.

In this paper, we firstly describe a low-temperature, cost effective, environment friendly method to synthesize a novel structure of $Li_{1.5}V_3O_8$ nanosheets. Nanosheet structure electrode materials exhibit both good capacity and cycling stability. The structure, morphology and electrochemical properties of the prepared $Li_{1.5}V_3O_8$ nanosheets were investigated. The correlation between the excellent electrochemical performance and the microstructure of $Li_{1.5}V_3O_8$ are reported.

2. Experimental

2.1. Materials preparation

$Li_{1.5}V_3O_8$ nanosheets were prepared by sol–gel method using the chemically pure $CH_3COOLi\cdot 2H_2O$, NH_4VO_3 and citric acid as the raw materials. A typical preparation process is as follow. First, NH_4VO_3 was dissolved in 75 ml distilled water with magnetic stirring. Then, $CH_3COOLi\cdot 2H_2O$ (The molar ratio of Li to V is 1:2.4.) was added, and the mixture was stirred for several minutes. Next, a stoichiometric amount of citric acid was added into the mixture. The color of the mixed solution changed slowly from salmon pink to clear blue. The resultant solution was heated at 80 °C until a dark blue gel formed. Subsequently, the obtained gel was dried at 110 °C in vacuum drying oven at least 12 h. The achieved precursor was calcined at 450 °C for 24 h under air. Then the $Li_{1.5}V_3O_8$ samples were obtained.

2.2. Characterization of sample

The structure of the prepared samples was determined by X-ray diffraction (XRD) using a PANalytical X-pert diffractometer with a Cu-Kα radiation operated at 40 kV and 30 mA. Hitachi field emission scanning electron microscopy (FE-SEM S-4800) measurement was used to observe the morphology. The details of the prepared samples were observed by transmission electron microscopy (TEM) (Hitachi, H-8100). The electrochemical properties of the materials were tested using CR2025 coin cells. The as-prepared powder was mixed in a weight ratio of 75 wt% of the as-prepared powder, 20 wt % of carbon black and 5 wt% of PVDF on aluminum foil. Then dried it in vacuum at 120 °C for 10 h. The typical active material loading was usually 1–2 mg cm^{-2}. The cells were assembled in argon-filled glove box (H_2O, $O_2 < 3$ ppm, Mikrouna, China). The electrolyte was the solution of 1 M $LiPF_6$ in a mixture of ethyl carbonate (EC)/dimethyl-carbonate (DMC) (1:1 volume ratio). Lithium metal was the anode and Celgard 2325 film was a separator. Charge–discharge testing was performed at different current densities between 1.5 and 4.0 V on a LAND CT-2000A cell test instrument. Cyclic voltammetry and electrochemical impedance were investigated in a two-electrode coin cell on an electrochemical station. CV tests were recorded between 1.5 and 4.0 V at a scanning rate of 0.1 mV s^{-1} vs. Li/Li^+ and EIS measurement was carried out in the frequency range from 100 kHz to 10 mHz and applying an AC signal of 5 mV.

3. Results and discussions

3.1. Structure

Fig. 1 shows the X-ray diffraction (XRD) pattern of the prepared $Li_{1.5}V_3O_8$. The diffraction peaks could be readily indexed into a monoclinic crystalline $Li_{1.5}V_3O_8$ (space group $P21/m$, JCPDS 86-2421) except for several impurity peaks of $Li_{1.2}V_9O_{22}$ and $Li_{1.5}V_{12}O_{29}$. It can be seen that this material is a mixed-phase vanadium oxide material, where the predominant phase is $Li_{1.5}V_3O_8$. It is composed of two basic structural units of VO_6 octahedron and VO_5 distorted trigonal bipyramids, which share corners with the octahedra. Li^+ ions can intercalate between these layers. The diffraction peak for the (−111) plane was sharpest suggesting that the layers of VO_n polyhedra had the largest dimension along (−111) plane. It is different from the known layered-type $Li_{1.5}V_3O_8$ (JCPDS 86-2421). This difference is also attributed to the preferred orientation of the $Li_{1.5}V_3O_8$ nanosheets structure.

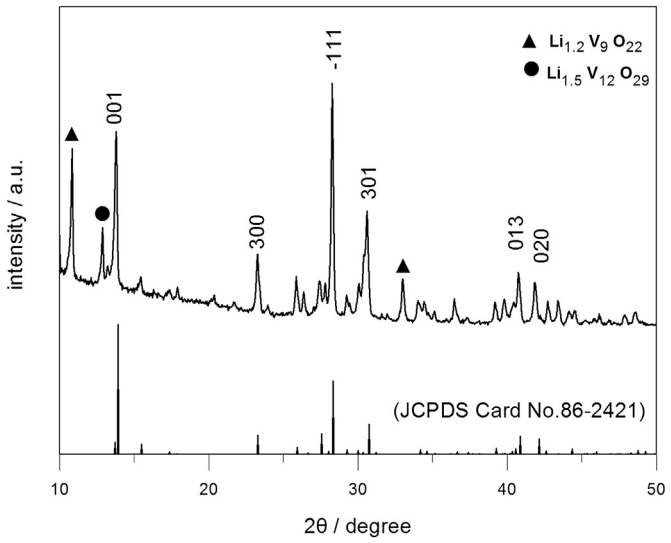

Fig. 1. XRD pattern of the as-prepared $Li_{1.5}V_3O_8$ calcined at 450 °C for 24 h under air.

3.2. Morphology

Fig. 2 shows SEM images of the as-prepared $Li_{1.5}V_3O_8$ with different magnifications (a), (b), (c) and TEM image of the $Li_{1.5}V_3O_8$(d). As shown in Fig. 2a, the unique nanosheet structure of the as-prepared $Li_{1.5}V_3O_8$ was clearly showed. In Fig. 2b, the as-prepared $Li_{1.5}V_3O_8$ exhibited a very long sheet-like morphology. Each sheet had smooth and clean surface. A higher magnification SEM image (shown in Fig. 2c) gave a clearer picture of the layered structure. The average thickness is about 25 nm. Each sheet was made up of several thin layers and the layer spacing was very short. The nanosheet structure was further confirmed by TEM images (shown in Fig. 2d), with a typical width of 600 nm and length of 800 nm. Very thin layers could be observed and at least four layers could be identified in Fig. 2d. The darker area (numbered '4') contained four layers, the dark area (numbered '3') contained three layers, the grey area (numbered '2') contained two layers and the bright area (numbered '1') contained one layer. This result is in good agreement with the SEM study, which shows the layer-by-layer stacking structures. This structure is quite unique in $Li_{1.5}V_3O_8$ and is different from the macaroni-like $Li_{1.2}V_3O_8$ described in other recent publication [19]. The structural change indicates that citric acid may play a key role in nanosheet structure formation. The space between each layer probably results from the decomposition of citric acid and the loss of residual carbon during the oxidation process in air. The study of the mechanism of nanosheet formation is under the way and will be reported later.

3.3. Electrochemical performance

Fig. 3a and b shows the initial charge–discharge curves and long-term cycling performance of $Li_{1.5}V_3O_8$ nanosheet electrodes at

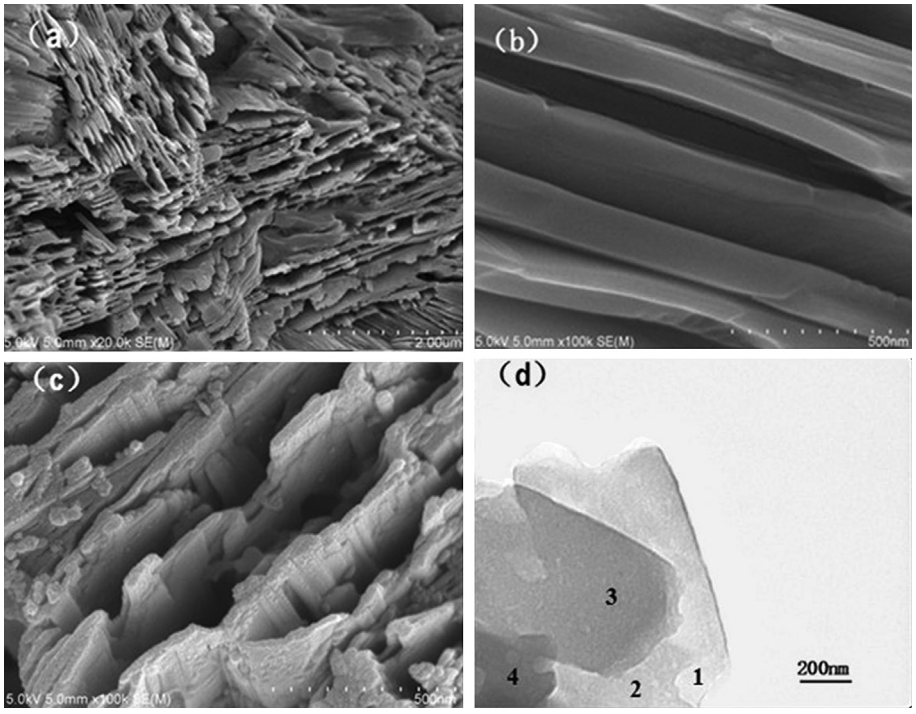

Fig. 2. SEM images of the as-prepared $Li_{1.5}V_3O_8$ with different magnifications (a), (b) and (c); TEM image of the $Li_{1.5}V_3O_8$ (d).

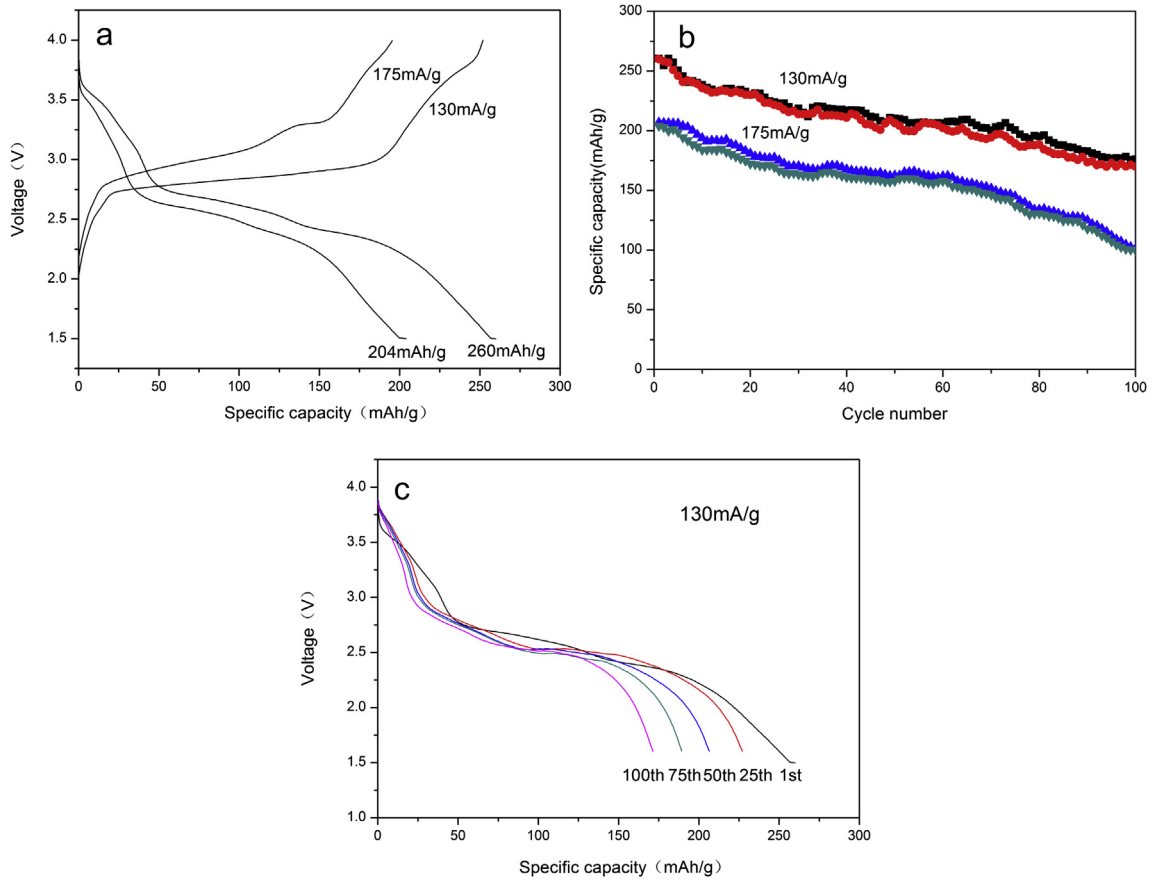

Fig. 3. Electrochemical performance of the $Li_{1.5}V_3O_8$/Li cells. (a) The initial charge–discharge curves at different current densities of 130 mA g^{-1} and 175 mA g^{-1}. (b) Long-term cycling performance of $Li_{1.5}V_3O_8$ nanosheets at different current densities of 130 mA g^{-1} and 175 mA g^{-1}. (c) The discharge curves at different cycles (1st, 25th, 50th, 75th, 100th) at 130 mA g^{-1}.

different current densities of 130 mA g^{-1} and 175 mA g^{-1}, respectively, when cycled between 1.5 and 4.0 V at room temperature. In Fig. 3a, it could be seen that all the discharge curves exhibited good voltage plateau. In the process of discharge, the voltage dropped obviously. It demonstrates that phase transitions may take place, but further test evidences are needed to explain this phenomenon [20]. The initial discharge specific capacity for the $Li_{1.5}V_3O_8$ electrode was 260 mAh g^{-1} at the current density of 130 mA g^{-1} (0.3 C). Whereas, at the current density of 175 mA g^{-1} (0.5 C), the discharge capacity was 204 mAh g^{-1}. W.Z. Wu reported single-crystalline LiV_3O_8 nanobelts had initial discharge specific capacity of 234 mAh g^{-1} at current density of 100 mA g^{-1} [21]. C. Cheng reported a macaroni-like $Li_{1.2}V_3O_8$ nanomaterial directly prepared through a facile solution route using cyclodextrn (β-CD) as a template reagent. Its initial discharge specific capacities were 189, 140 mAh g^{-1} at 0.1 C, 0.5 C, respectively [19]. The rods synthesized by Sakunthala et al. reported good cycle stability and moderate specific discharge capacities of 230, 180 mAh g^{-1} at current densities of 30 mA g^{-1} and 120 mA g^{-1}, respectively [22]. H. Wang also reported nanosheet structure electrode prepared by hydrothermal method, which has good discharge capacity (compared with present report) of 260.0, 232.4, 173.9 and 148.7 mAh g^{-1} at 0.4, 1.0, 3.0 and 5.0 C (1C = 300 mA g^{-1}), respectively [18]. Compared with these results [18,19,21–23], it can be seen that the morphology of electrodes have great effect on electrochemical properties. The $Li_{1.5}V_3O_8$ nanosheet electrodes have higher initial discharge specific capacity, which might be attributed to the nano-layer structure and the extra lithium content of the plat-like $Li_{1.5}V_3O_8$ nanomaterial. Due to its special nanostructure, the as-prepared $Li_{1.5}V_3O_8$ material can be easily filled with the electrolyte, ensuring a relatively high surface area being in contact with the electrolyte, and then provide lithium ions with more sites. On the other hand, the short spacing of layers is good for the Li^+ ion diffusion process, because it saves the time of the diffusion process. As a result, many lithium ions can immediately insert into and extract from the electrode materials during the electrochemical reaction. Consequently, the as-prepared $Li_{1.5}V_3O_8$ nanosheets displayed high discharge specific capacity in the electrolyte.

In Fig. 3b, it can be seen that the discharge capacity reached to 170 mAh g^{-1} remaining 65.3% of the initial capacities at a current density of 130 mA g^{-1} after 100 cycles. When the current density was increased to 175 mA g^{-1}, its discharge capacity still reached to 100 mAh g^{-1} remaining 49% of the initial capacity after 100 cycles. The macaroni-like $Li_{1.2}V_3O_8$ nanomaterial delivered capacities of 68, 53 mAh g^{-1} at 0.1, 0.5 C, respectively, remaining 36%, 38% of the initial capacities after 100 cycles [19]. It can be seen that the $Li_{1.5}V_3O_8$ nanosheets showed better cycle performance. The charge–discharge cycle curves were nearly approaching, respectively. It means that the transformation efficiency of charge and discharge is relatively high. A small drop was found in the discharge capacity during the first 30 cycles, which might be ascribed that some lithium ions cannot be completely inserted and extracted from the $Li_{1.5}V_3O_8$ structure. The capacity loss observed on $Li_{1.5}V_3O_8$ was about 19.5% and 19.8% at different current densities of 130 mA g^{-1} and 175 mA g^{-1} during the first 30 cycles. But capacity loss became slow along with cycles. After the 30th cycle, the capacity retention was kept about 97.5% and 97.1%, respectively. The capacity became relatively stable in the further cycles and finally reached the high capacities of 194.4 mAh g^{-1} and 146.4 mAh g^{-1}, respectively in the70th cycle. After 70 cycles, the fading in electrochemical performance of $Li_{1.5}V_3O_8$ nanosheets was not obvious. The discharge curves of $Li_{1.5}V_3O_8$ nanosheet electrodes at different cycles (1st, 25th, 50th, 75th, 100th) were shown in Fig. 3c. It indicates that the voltage plateau between 2.37 and 2.48 V decreased slightly with the increasing of cycles. Moreover, it was noticeable that the capacity loss within the plateau from 2.53 to 2.65 V was much larger than others. It could be deduced that $Li_{1.5}V_3O_8$ possesses poorer reversible ability for lithium insertion/extraction within the voltage plateau of 2.56 V, which is considered as a main reason for capacity fading.

Fig. 4 shows consecutive cyclic behavior of the as-prepared $Li_{1.5}V_3O_8$ electrode at different current densities of 40, 85, 130, 175, 310, 625 mA g^{-1}. In the first 10 cycles, at the current density of 40 mA g^{-1}, the initial charge and discharge specific capacity was 283.6 mAh g^{-1} and 280.6 mAh g^{-1}, but the capacity loss was obvious with cycle number. The low efficiency at low current density agreed well with the relatively poor cycling performance, which was very common for vanadates [23]. After 10 cycles, it could be observed that the capacity increased with cycle number. The reason of this phenomenon may be that the lithium ions could not be able to take part in the initial cycling, but with the cycle number increasing, more active material may be able to participate because of electrochemical grinding. Another reason may be the slight fragmentation of the grains. The smaller grain size reduces the diffusion path for the lithium ions [24]. Except for those first 10 cycles, no obvious capacity fading was found at low current density. But with the increasing of current density, the capacity declined. It may be attributed to the fact that more available sites for Li^+ could be used at low current density, some of which probably possess the inferior reversibility of Li ions insertion and extraction. While cycling at high current density, those sites could not be used because of the fast insertion and extraction. After 60 cycles, even at high current density of 625 mA g^{-1}, the cell retained an initial discharge specific capacity of 120 mA h g^{-1}. After 100 cycles, the electrode still had a discharge specific capacity of 88.4 mA h g^{-1}. It had been reported good rate properties and cycling properties also by A Pan. They obtained a discharge specific capacity of 120 mA h g^{-1} at a 1 C charging rate (140 mA g^{-1}), and the discharge specific capacity was 118 mAh g^{-1} when operated at 4 C [25]. For our $Li_{1.5}V_3O_8$ electrode, at high current density of 175 mA g^{-1}, it had the discharge capacity of 194 mA h g^{-1}. When operated at high current density of 625 mA g^{-1}, it had the discharge capacity of 120 mA h g^{-1}. It can be seen that our $Li_{1.5}V_3O_8$ electrode showed excellent rate performance and good capacity retention (shown in Fig. 4), which is attributed to the novel structure of the $Li_{1.5}V_3O_8$. The nanosheets reduce the diffusion distance for lithium ions, which induces good conductivity of the active material.

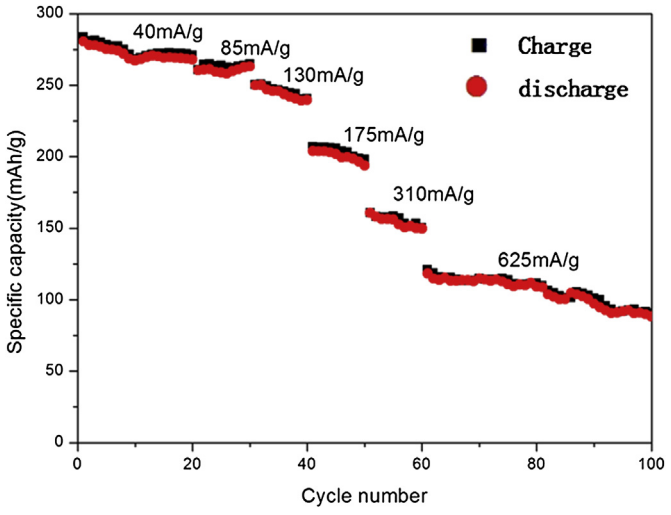

Fig. 4. Consecutive cyclic behavior at different current densities.

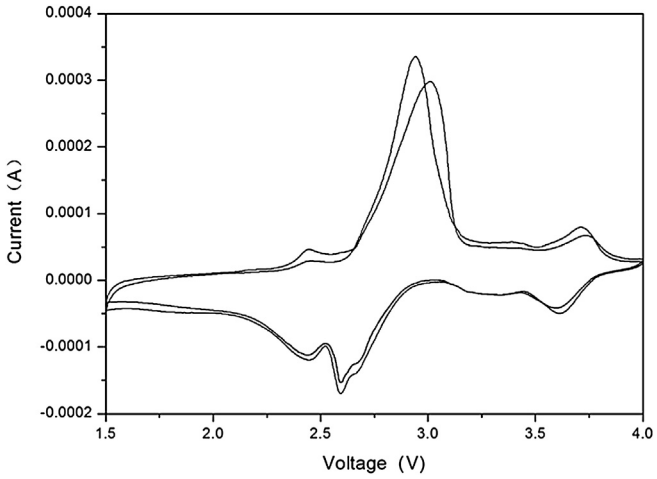

Fig. 5. Cyclic voltammetry curves of $Li_{1.5}V_3O_8$ nanosheets between 1.5 and 4.0 V at a scanning rate of 0.1 mV s^{-1}.

Fig. 5 shows CV curves of $Li_{1.5}V_3O_8$ nanosheets. Highly reversible lithium ion insertion/extraction ability was indicated. Three obvious peaks at 2.45, 2.87 and 3.70 V were observed in the anodic scan. While more peaks at 2.44, 2.56, 2.68 and 3.63 V appeared, indicating the multi-steps lithium insertion/extraction processes. The CV curves corresponded well with the charge/discharge plateaus (shown in Fig. 3a) and almost superimposed over each other, except for a very small difference observed at 2.87 V and 2.56 V. The splitting of many redox peaks is because of the different lithium sites with energy difference for lithium ions holding [26]. The well-observed peaks in our experiment are largely attributed to the novel nanosheet-structures. As shown in Fig. 2c, the space between nanosheets is short, which facilitates the electrolyte penetration and reduces the energy barrier for Li^+ ion insertion/extraction. Therefore the phase change can happen rapidly. The complicated lithium ion insertion/extraction processes are very common for other vanadate compounds, such as V_2O_5 [27,28], $Na_2V_6O_{16}\cdot xH_2O$ [29–31] and $NH_4V_3O_8$ [32,33] etc. The good agreement of the CV curves demonstrates good structural reversibility and good cycle stability for the $Li_{1.5}V_3O_8$ electrode.

Fig. 6 shows the electrochemical impedance spectra of the sample after 1, 5 and 10 cycles. The impedance plot was fitted using the equivalent circuit model shown in the inset, where C_{DL} represented the double layer capacitance. The Nyquist plot showed a semicircle in the high to medium frequency range, which described the charge-transfer resistance (R_{ct}) for the electrode. The intercept value represented the total electrical resistance offered by the electrolyte (R_s). The inclined line represented the Warburg impedance (Z_w) at low frequency, which showed the diffusion of Li^+ in the solid matrix. As was shown in Fig. 6, with the cycle number increasing, the resistance of cell firstly increased and then decreased, which was consistent with the capacity changing trend. The resistance is related to various process, which depends on the electrode materials, for instance, active materials dissolution, passive film formation, or loss of electrical contact, etc. All the above processes might be involved in the initial state of the present work, and induced the resistance increase in the first few cycles. After 10 cycles, the resistance of the cell decreased to 140Ω, possibly because of the processes of activation and stabilization existing in the electrode materials. This lower resistance indicates that charge-transfer is easier in nanosheet electrodes. The enough space between the layers facilitates electrolyte penetration and increases the interfacial contact area between electrolyte and electrode. Because the electron transportation distance is reduced in nanoscale materials, electrons can transfer effectively. Therefore, nanosheet structure improved the battery performance on high capacity and good cycling as the resistance decreased.

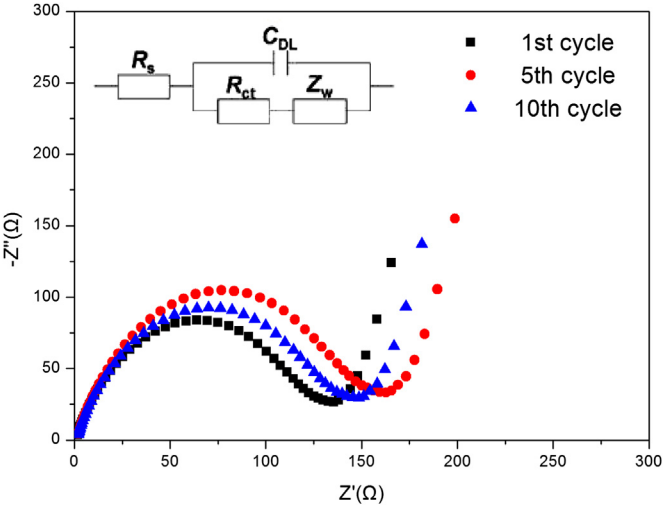

Fig. 6. Electrochemical impedance spectra of the sample for cycles at 1st, 5th and 10th. The equivalent circuit (inset) was used for fitting the EIS spectra.

4. Conclusions

$Li_{1.5}V_3O_8$ nanosheets were prepared by sol–gel method. The as-prepared material showed high discharge specific capacity and good cycling stability with discharge specific capacity of 260, 204 mAh g^{-1} at current densities of 130 mA g^{-1} and 175 mA g^{-1}. After 100 cycles, its discharge capacity still maintained at 170 mAh g^{-1} and 100 mAh g^{-1}. The good performance can be ascribed to nanosheet structure, which shortens the diffusion paths of lithium ions, decreases charge-transfer resistance and increases large surface area. It can be expected that $Li_{1.5}V_3O_8$ nanosheets may be a promising candidate materials for lithium-ion batteries.

Acknowledgment

This work was supported by National Natural Science Foundation of China (Grants 50972017).

References

[1] M. Armand, J.M. Tarascon, Nature 451 (2008) 652–657.
[2] J.X. Dai, S.F.Y. Li, Z.Q. Gao, K.S. Siow, J. Electrochem. Soc. 145 (1998) 3057–3062.
[3] K. West, B. Zachauchristiansen, S. skaarup, Y. Saidi, J. Barker, I.I. Olsen, R. Pynenburg, R. Loksbang, J. Electrochem. Soc. 143 (1996) 820–825.
[4] H.Y. Xu, H. Wang, Z.Q. Song, Y.W. Wang, H. Yan, M. Yoshimura, Electrochim. Acta 49 (2004) 349–353.
[5] E.S. Takeuchi, K.J. Takeuchi, A.C. Marschilok, Encyclopedia of Electrochemical Power Sources, Elseiver, Amsterdam, 2009, pp. 100–110.
[6] L.A. Picciotto, K.T. Adendorff, D.C. Liles, M.M. Thackeray, Solid State Ionics 62 (1993) 297–307.
[7] G. Pistoia, S. Panero, M. Tocci, R.V. Moshtev, V. Manev, Solid State Ionics 14 (1984) 311–318.
[8] G. Pistioa, M. Pasquali, M. Tocci, R.V. Moshtev, V. Maner, J. Electrochem. Soc. 132 (1985) 281–284.
[9] N. Tran, K.G. Bramnik, H. Hibst, J. Prölß, N. Mronga, M. Holzapfel, W. Scheifele, P. Novák, J. Electrochem. Soc. 155 (2008) A384–A389.
[10] G. Yang, G. Wang, W. Hou, J. Phys. Chem. B 109 (2005) 11186–11196.
[11] Q. Liu, H. Liu, X. Zhou, C. Cong, K. Zhang, Solid State Ionics 176 (2005) 1549–1554.
[12] M. Dubarry, J. Gaubicher, D. Guyomard, Chem. Mater. 17 (2005) 2276–2283.
[13] A.C. Marschilok, C.P. Schaffer, K.J. Takeuchi, E.S. Takeuchi, J. Composite Mater. 47 (2013) 41–49.

[14] C. Sanchez, L. Rozes, F. Ribot, C. Laberty-Robert, D. Grosso, C. Sassoye, C. Boissiere, L. Nicole, Comptes Rendus Chim. 13 (2010) 3–39.
[15] A. Pan, J. Liu, J.G. Zhang, G. Cao, W. Xu, Z. Nie, X. Jie, D. Choi, B.W. Arey, C. Wang, S. Liang, J. Mater. Chem. 21 (2011) 1153–1161.
[16] C.J. Cui, G.M. Wu, J. Shen, B. Zhou, Z.H. Zhang, H.Y. Yang, S.F. She, Electrochim. Acta 55 (2010) 2536–2541.
[17] A.Q. Pan, J.G. Zhang, G.Z. Cao, J. Mater. Chem. 21 (2011) 10077–10084.
[18] H. Wang, Y. Ren, Y. Wang, CrystEngComm 14 (2012) 2831–2836.
[19] C. Cheng, Z.H. Li, X.Y. Zhan, Electrochim. Acta 55 (2010) 4627–4631.
[20] G.Q. Liu, C.L. Zeng, K. Yang, Electrochim. Acta 47 (2002) 3239–3243.
[21] W.Z. Wu, J. Ding, H.G. Peng, G.C. Li, Mater. Lett. 65 (2011) 2155–2157.
[22] A. Sakunthala, M.V. Reddy, B.V.R. Chowdari, P.C. Selvin, J. Phys. Chem. C 114 (2010) 8099–8107.
[23] H.M. Liu, Y.G. Wang, K.X. Wang, Y.R. Wang, H.S. Zhou, J. Power Sources 192 (2009) 668–673.
[24] Y. Liu, X. Zhou, Y. Guo, Electrochim. Acta 54 (2009) 3184–3190.
[25] A.Q. Pan, J. Liu, J.G. Zhang, Electrochem. Commun. 12 (2010) 1674–1677.
[26] J. Kawakita, M. Majima, T. Miura, T. Kishi, J. Power Sources 66 (1997) 135–139.
[27] A.M. Cao, J.S. Hu, H.P. Liang, L.J. Wan, Angew. Chem. Int. Ed. 44 (2005) 4391–4395.
[28] J. Livage, Chem. Mater. 3 (1991) 578–593.
[29] H.Y. Wang, W.J. Wang, Y. Ren, K.L. Huang, S.Q. Liu, J. Power Sources 199 (2012) 263–269.
[30] C.Y. Lee, A.C. Marschilok, A. Subramanian, K.J. Takeuchi, E.S. Takeuchi, Phys. Chem. Chem. Phys. 13 (2011) 18047–18054.
[31] A.C. Marschilok, C.Y. Lee, A. Subramanian, K.J. Takeuchi, E.S. Takeuchi, Energy Environ. Sci. 4 (2011) 2943–2951.
[32] H.Y. Wang, K.L. Huang, S.Q. Liu, C.H. Huang, W.J. Wang, Y. Ren, J. Power Sources 196 (2011) 788–792.
[33] H.Y. Wang, K.L. Huang, Y. Ren, X.B. Huang, S.Q. Liu, W.J. Wang, J. Power Sources 196 (2011) 9786–9791.